Article:
Chen, Q., Xia, Y., Wang, J. orcid.org/0000-0003-4870-3744 et al. (2 more authors) (2022) Short-circuit fault-tolerant control for five-phase fault-tolerant permanent magnet motors with trapezoidal back-EMF. Fundamental Research, 2 (6). pp. 964-973. ISSN 2667-3258

https://doi.org/10.1016/j.fmre.2021.09.009

Fundamental Research xxx (xxxx) xxx

Contents lists available at ScienceDirect

Fundamental Research

journal homepage: http://www.keaipublishing.com/en/journals/fundamental-research/

Article

Short-circuit fault-tolerant control for five-phase fault-tolerant permanent magnet motors with trapezoidal back-EMF

Qian Chen[a], Yuhang Xia[a], Jiabin Wang[b], Wenxiang Zhao[a,*], Guohai Liu[a]

[a] School of Electrical and Information Engineering, Jiangsu University, Zhenjiang 212013, China
[b] Department of Electronic and Electrical Engineering, The University of Sheffield, Sheffield S1 3JD, UK

ARTICLE INFO

Keywords:
Short-circuit fault
Five-phase fault-tolerant permanent magnet synchronous motor
Trapezoidal back electromotive force
Fault-tolerant
Deadbeat current predictive control

ABSTRACT

When a short-circuit fault occurs in a phase, the faulty phase needs to be removed artificially from the system because of the loss of the capability to generate torque. In this case, both the short-circuit current and phase-loss fault would generate additional torque ripples. In this study, a novel fault-tolerant control strategy is introduced to achieve low torque ripple operation of five-phase fault-tolerant permanent magnet synchronous motors with trapezoidal back electromotive force (FTPMSM-TEMF) in the event of a short-circuit fault. The key concept of this method is to compensate for the torque ripples caused by the short-circuit current and the adverse effect of the phase-loss. Based on the torque expression under fault conditions, the torque ripple caused by the short-circuit current can be offset by injecting a certain pulsating component into the torque expression in the phase-loss condition. This would result in smooth operation under fault conditions. Moreover, to track the fault-tolerant alternating currents, the model of the deadbeat current predictive control is extended and restructured for the fault condition. The effectiveness and feasibility of the proposed fault-tolerant strategy are verified by experimental results.

1. Introduction

The peak value of the air gap magnetic density of five-phase fault-tolerant permanent magnet synchronous motors with trapezoidal back electromotive force (FTPMSM-TEMF) can be reduced effectively by injecting a specific ratio of third harmonic currents. Thereby, the utilization rate of the core material and the output torque of the motor can be improved [1]. Meanwhile, a five-phase FTPMSM-TEMF can provide high output torque and display a high fault-tolerance capability compared with conventional three-phase motors because of the additional degrees of freedom. Owing to the higher degrees of freedom of the motor [2], the adoption of an effective fault-tolerant control method would enable the remaining healthy phases to suppress the impact of the faulty phase and deliver a smooth torque without additional hardware [3]. However, when a single-phase short-circuit fault occurs, more torque ripples would be generated because of the presence of trapezoidal back electromotive force (back-EMF). This would eventually result in more severe operations under fault conditions. Meanwhile, because more pulsation components need to be considered, it would further hinder fault-tolerant control.

During the fault-tolerant operation of the multi-phase motor, the currents of the remaining healthy phases have to be rearranged to adapt to the fault conditions. The general criteria for current reconstruction after failure are to maintain a fundamental magnetic motive force (MMF) equal to that in the healthy condition [4–7]. Tian B and Liu G proposed the decoupling matrices at the fundamental [8] and third harmonic [9] spaces to maintain the back-EMF unaltered pre- and post-fault. However, these methods were proposed only for open-circuit faults. Stator-related faults have been reported to be common in electrical motors, accounting for 21–37% of the total motor failures [10]. Meanwhile, inter-turn short-circuit is the most common winding fault that accompanies a large short-circuit current. The short-circuit current would result in an abrupt increase in temperature and continuously destroy the winding insulation. In certain high-reliability occasions, it is infeasible to replace the faulty motor immediately. Eventually, the complete loss of insulation would result in a short-circuit fault of the entire phase. Unlike an inter-turn short-circuit, the plus-width modulation (PWM) signal of the faulty phase's leg of the voltage source inverter would be turned off artificially owing to the loss of the faulty phase's capability to output torque. Hence, the faulty phase would be disconnected from the source. This type of fault is more severe and hazardous [11–14] because both asymmetrical four phases and short-circuit current would generate additional torque ripples. Extensive research has been performed on short-circuit faults [16–22] to enhance the operational performance under short-circuit fault conditions [15]. A remedial phase-angle control strategy based on short-circuit current [16] was proposed by limiting reactive components of the torque ripple. However, the short-circuit current

* **Corresponding author**.
E-mail address: zwx@ujs.edu.cn (W. Zhao).

https://doi.org/10.1016/j.fmre.2021.09.009
Received 30 April 2021; Received in revised form 30 August 2021; Accepted 18 September 2021
Available online xxx

Please cite this article as: Q. Chen, Y. Xia, J. Wang et al., Short-circuit fault-tolerant control for five-phase fault-tolerant permanent magnet motors with trapezoidal back-EMF, Fundamental Research, https://doi.org/10.1016/j.fmre.2021.09.009

was obtained by simulation, which caused errors and limited practicality. By collecting short-circuit current online, compensatory reference currents were proposed in [17] to eliminate the effect of short-circuit current. However, this method needs to cooperate with additional compensatory voltages and is not suitable for permanent magnet (PM) motors with trapezoidal back electromotive force (EMF). For similar motors, Wu F analyzed the modeling of short-circuit current and the influence of third harmonic back-EMF for open-winding PM motors [18]. Based on an analysis of the torque ripple caused by a short-circuit current, feed-forward control was employed in [19] to reduce the torque ripple. However, the influence of short-circuit current cannot be suppressed completely owing to the use of the direct torque control (DTC) method. To produce ripple-free torque with minimum ohmic loss, an online optimal current reference generation technique based on the Lagrange multiplier method was presented in [20–22] based on the Lagrange multiplier method. However, the process of determination of the optimal solution is carried out in the natural coordinate system, which requires complex calculations. Meanwhile, the influence of the motor failure is not fully utilized and is equivalent to a disturbance.

In these single-phase short-circuit fault-tolerant control methods, the reference currents in the synchronous rotating coordinate system are alternating current (AC) quantities, which are difficult to track by the conventional proportional-integral (PI) controller. A hysteresis current controller is typically employed for alternating signals [20,21]. However, it would result in a variable switching frequency, an increase in switching loss, and electromagnetic interference emission. The proportional resonant (PR) controller is another solution for tracking time-varying signals [22–24]. However, the control references are time-varying with higher-order harmonics, rather than constants. This significantly hinders controller design. Deadbeat current prediction control is another method to track AC quantities (except for the hysteresis current controllers and PR controllers) [25–27]. However, most deadbeat current prediction control is constructed based only on a normal condition. A deadbeat predictive current control [28] method was proposed for inverter failure. However, the model of the motor is in the normal state.

The amplitude of the short-circuit current would decrease with an increase in the short-circuit turn [29]. Meanwhile, the motor used in this study is a fault-tolerant motor [30]. It displays both higher self-inductance and lower mutual inductance. The higher self / mutual inductance ratio is favorable for restricting the short-circuit current [31] (can be limited to below two times of the rated current). In addition, to prevent the propagation of the short-circuit fault to healthy phases, alternate-teeth wound fractional-slot concentrated-windings and fault-tolerant teeth have been adopted to achieve electrical, mechanical, thermal, and magnetic isolation between phases. Thus, if the PM motor adopts a fault-tolerant design, the phase short-circuit fault would not destroy the motor rapidly. However, when a short-circuit occurs, the faulty phase's winding would become disconnected from the source artificially owing to the fault-tolerant strategy. In this case, both asymmetrical four phases and short-circuit current would generate additional torque ripples. Furthermore, the torque ripples increase with the number in short-circuit turns [32].

Thus, the objective of this study is to maintain the average torque and reduce the torque ripple for a five-phase FTPMSM-TEMF in the case of a single-phase short-circuit. The main contributions of the study are as follows: (1) The adverse effects of a short-circuit fault can be divided into two parts: the phase-loss and additional torque ripple caused by the short-circuit current. The proposed fault-tolerant strategy fully utilizes these effects by injecting the fault-tolerant currents in the fundamental and third harmonic spaces. The phase-loss fault would generate additional torque ripples, which can be utilized to offset the ripple caused by the short-circuit current. (2) Because the fault-tolerant reference currents are AC quantities in the synchronous rotating coordinate system, a deadbeat current prediction method combined with carrier pulse width modulation (CPWM) is proposed. The proposed deadbeat method can track the alternating singles and replace the PI controller of the closed-loop current. This simplifies the control structure. Meanwhile, owing to the use of the CPWM generator, the switching frequency can be maintained in a stable state, and the computational burden of the system can be reduced.

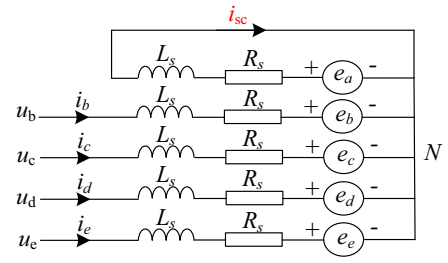

Fig. 1. Schematic diagram of short-circuit fault in Phase A.

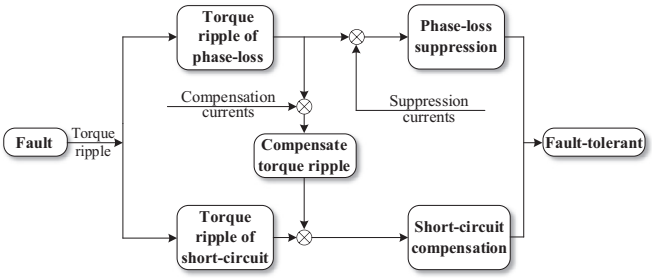

Fig. 2. Flow diagram of fault tolerance.

2. Fault-tolerant strategy for short-circuit

When Phase A undergoes short-circuit fault, it loses the capability to output torque. Therefore, the PWM signal of the faulty phase would be turned off artificially. This is equivalent to winding disconnection from the source [17, 22]. Fig. 1 shows a schematic diagram of the short-circuit fault of Phase A. Here, i_{sc} is the short-circuit current of Phase A; i_b, i_c, i_d, and i_e are healthy phase currents; and e_a, e_b, e_c, e_d, e_e represent the back-EMF of each phase. Meanwhile, a short-circuit current would be generated owing to the presence of the back-EMF. As shown in Fig. 2, there are two adverse effects of the fault condition: the effect of the loss of Phase A and the effect of the short-circuit current. If the influence of the short-circuit current can be offset by additional compensation currents, the model under short-circuit fault would be equivalent to a phase-loss fault. Thus, a mathematical model of the five-phase FTPMSM-TEMF under a short-circuit fault can be established similarly as that under a phase-loss fault.

2.1. Suppress the effect of phase-loss

A new set of Clarke and Park transformations is developed for disturbance-free operation under phase-loss fault conditions. The decoupled modeling is based on the maintenance of the spatial circular rotation of the fundamental PM flux linkage vector and magnetomotive force. The Clarke and Park transformations under fault conditions can be described as follows [8]:

$$\boldsymbol{T}^{A}_{park1} = \begin{bmatrix} \cos\theta & \sin\theta & 0 & 0 \\ -\sin\theta & \cos\theta & 0 & 0 \\ 0 & 0 & 1 & 0 \\ 0 & 0 & 0 & 1 \end{bmatrix} \tag{1}$$

$$\boldsymbol{T}^{A}_{clarke1} = \frac{2}{5}\begin{bmatrix} \cos a - 1 & \cos 2a - 1 & \cos 2a - 1 & \cos a - 1 \\ \sin\alpha & \sin 2\alpha & -\sin 2\alpha & -\sin\alpha \\ -\sin 2\alpha & \sin\alpha & -\sin\alpha & \sin 2\alpha \\ 1/2 & 1/2 & 1/2 & 1/2 \end{bmatrix} \tag{2}$$

where $\boldsymbol{T}^{A}_{clarke1}$ and $\boldsymbol{T}^{A}_{park1}$ represent the fundamental reduced-order Clarke and Park transformations, respectively, under Phase-A fault; θ is the electrical angle of the rotor position of the motor; and $\alpha = 0.4\pi$.

Taking a derivative of magnetic co-energy to the rotor mechanical position and omitting the magnetic saturation effect, the torque equation can be obtained as:

$$T_e = P(\frac{1}{2}\boldsymbol{I}_s^T \frac{\partial \boldsymbol{L}_s}{\partial \theta}\boldsymbol{I}_s + \boldsymbol{I}_s^T \frac{\partial \boldsymbol{\psi}_s}{\partial \theta}) \tag{3}$$

where P is the number of motor pole-pairs, $\boldsymbol{I}_s$ indicates the current vector, and $\boldsymbol{L}_s$ is the reduced-order inductance matrix from which the elements related to the faulty phase are removed. $\boldsymbol{\Psi}_s$ presents the PM flux linkage matrix as shown in Eq. 4:

$$\boldsymbol{\psi}_s = \psi_1 \begin{bmatrix} \cos(\theta-\alpha) \\ \cos(\theta-2\alpha) \\ \cos(\theta-3\alpha) \\ \cos(\theta-4\alpha) \end{bmatrix} + \psi_3 \begin{bmatrix} \cos 3(\theta-\alpha) \\ \cos 3(\theta-2\alpha) \\ \cos 3(\theta-3\alpha) \\ \cos 3(\theta-4\alpha) \end{bmatrix} \tag{4}$$

where Ψ_1 and Ψ_3 denote the amplitudes of the fundamental and third harmonic PM flux linkage, respectively.

By substituting Eq. 4 into Eq. 3, the electromagnetic torque at the fundamental synchronous rotating coordinate can be obtained as Eq. 5. The detailed process is presented in the appendix.

$$\begin{aligned} T_{e1} = \frac{5P}{2}\{&(L_{d1}-L_{q1})i_{d1}i_{q1} + \psi_1 i_{q1} + 3\psi_3[0.5i_{d1}(\sin 2\theta + \sin 4\theta) \\ &- 0.5i_{q1}(\cos 2\theta - \cos 4\theta) + i_{z1}\cos 3\theta]\} \end{aligned} \tag{5}$$

where L_{d1} and L_{q1} are the inductance component in the fundamental synchronous rotating coordinate. Its calculation method is presented in the appendix. i_{d1} and i_{q1} denote the fundamental synchronous rotating currents at the $d1$-$q1$ axis, respectively, and i_{z1} represents the third harmonic current in a fundamental synchronous rotating coordinate.

The Park transformation for the third harmonic space is expressed as Eq. 6. Similarly, the method can be utilized to obtain the torque expression at the third harmonic synchronous rotating coordinate [9]. This is illustrated in Eq. 7:

$$\boldsymbol{T}^{A}_{clarke3} = \frac{2}{5}\begin{bmatrix} \cos 2\alpha - 1 & \cos\alpha - 1 & \cos\alpha - 1 & \cos 2\alpha - 1 \\ -\sin 2\alpha & \sin\alpha & -\sin\alpha & \sin 2\alpha \\ \sin\alpha & \sin 2\alpha & -\sin 2\alpha & -\sin\alpha \\ 1/2 & 1/2 & 1/2 & 1/2 \end{bmatrix} \tag{6}$$

$$\begin{aligned} T_{e3} = \frac{5P}{2}\{&(L_{d3}-L_{q3})i_{d3}i_{q3} + 3\psi_3 i_{q3} + \psi_1[0.5i_{d3}(\sin 4\theta - \sin 2\theta) \\ &+ 0.5i_{q3}(\cos 4\theta - \cos 2\theta) + i_{z3}\cos\theta]\} \end{aligned} \tag{7}$$

where i_{d3} and i_{q3} indicate the third harmonic synchronous rotating currents at the $d3$-$q3$ axis, respectively, and i_{z3} is the fundamental current in a third harmonic synchronous rotating coordinate.

Owing to the loss of the faulty phase, the torque expressions generated by the currents in the remaining healthy phase are different from those for the normal condition. It is evident from Eqs. 5, 7 that when phase-loss occurs, the remaining healthy phase would develop an average torque as well as first-, second-, third-, and fourth-order torque ripples. The suppression currents should be allocated as follows to suppress the pulsation caused by the phase-loss in the fundamental and third harmonic space:

$$i_{d1o} = 0, i_{d3o} = 0, i_{q3o} = -\frac{3\psi_3}{\psi_1}i_{q1o}, i_{z3o} = -3\frac{\psi_3}{\psi_1}i_{z1o}\frac{\cos 3\theta}{\cos\theta} \tag{8}$$

where i_{d1o}, i_{q1o}, i_{d3o}, i_{q3o}, i_{z1o}, and i_{z3o} represent the reference currents that are utilized to suppress the torque ripples caused by phase-loss. i_{q1o} is generated by the PI controller of the speed closed-loop.

The torque ripple of each order can be suppressed completely by utilizing the reference currents proposed above, and only the average torque would exist. However, a degree of freedom i_{z1o} remains, which can be set to zero to minimize copper loss. The influence of the phase-loss can be suppressed when the reference currents satisfy the above conditions.

2.2. Compensate the effect of short-circuit current

As shown in Fig. 2, after the suppression of the influence of the phase-loss, the only impact on the motor is the short-circuit current. In this list, the effect on the motor caused by the phase-loss is utilized to compensate for the influence of the short-circuit current.

It is evident from Fig. 1 that when a short-circuit fault occurs in Phase A, the back-EMF would generate an additional torque ripple as shown in Eq. 9:

$$T_{sc} = \frac{e_a i_{sc} P}{\omega} = -i_{sc}P\left[\psi_1 \sin\theta + 3\psi_3 \sin 3\theta\right] \tag{9}$$

where ω is the electrical angular velocity of the rotor. It satisfies the relationship $\theta = \omega t$. i_{sc} is the short-circuit current of Phase A, which is monitored in real-time. e_a denotes the back-EMF of Phase A as follows:

$$e_a = \frac{d\psi_A}{d_t} = \frac{d\left[\psi_1\cos(\omega t) + \psi_3\cos(3\omega t)\right]}{dt} = -\omega\psi_1\sin(\omega t) - 3\omega\psi_3\sin(3\omega t) \tag{10}$$

It is evident from Eq. 9 that the short-circuit current interacts with the back-EMF and then generates first- and third-order torque ripples. This would influence the smooth operation of the motor under the short-circuit condition.

Owing to the loss of Phase A, the remaining healthy phases can develop an additional torque ripple. From Eqs. 5, 7, when the compensation currents are injected into the normal phase with the first-order ripple component, the second- and fourth-order torque ripples would be converted into first- and third-order ripples. This can be utilized to compensate the influence of the short-circuit current. The compensation currents can be assumed as shown:

$$\begin{aligned} &i_{d1s} = A\cos(\theta), i_{d3s} = -\frac{3\psi_3}{\psi_1}B\cos(\theta), i_{q1s} = B\sin(\theta), i_{q3s} = -\frac{3\psi_3}{\psi_1}A\sin(\theta), \\ &i_{z1s} = C\sin(\theta), i_{z3s} = -\frac{3\psi_3}{\psi_1}C\sin(3\theta) \end{aligned} \tag{11}$$

where A, B, and C are the amplitudes of the compensation currents; and i_{d1s}, i_{q1s}, i_{d3s}, i_{q3s}, i_{z1s}, and i_{z3s} represent the compensation currents in the synchronous rotating coordinate.

By substituting Eq. 11 into the torque expression Eqs. 5, 7, the compensated torque in the fundamental and third harmonic spaces can be obtained as shown in Eqs. 12, 13, respectively:

$$\begin{cases} T_{11} = \frac{5P}{2}\psi_1 B\sin\theta, T_{12} = \frac{15P}{4}\psi_3 A\sin 2\theta\cos\theta, T_{13} = \frac{15P}{4}\psi_3 A\sin 4\theta\cos\theta, \\ T_{14} = -\frac{15P}{4}\psi_3 B\cos 2\theta\sin\theta \\ T_{15} = \frac{15P}{4}\psi_3 B\cos 4\theta\sin\theta, T_{16} = \frac{30P}{4}\psi_3 C\cos 3\theta\sin\theta, \\ T_{17} = \frac{5P}{4}(L_{d1}-L_{q1})AB\sin 2\theta \end{cases} \tag{12}$$

where T_{1x} and x ∈ (1,2,3,4,5,6,7) are the fundamental electromagnetic compensated torque.

$$\begin{cases} T_{31} = -\frac{45P}{2}\frac{\psi_3^2}{\psi_1}A\sin\theta, T_{32} = \frac{15P}{4}\psi_3 A\cos 2\theta\sin\theta, T_{33} = -\frac{15P}{4}\psi_3 A\cos 4\theta\sin\theta, \\ T_{34} = \frac{15P}{4}\psi_3 B\sin 2\theta\cos\theta \\ T_{35} = -\frac{15P}{4}\psi_3 B\sin 4\theta\cos\theta, T_{36} = -\frac{15P}{2}\psi_3 C\sin 3\theta\cos\theta, \\ T_{37} = \frac{45P}{4}(L_{d3}-L_{q3})\frac{\psi_3^2}{\psi_1^2}AB\sin 2\theta \end{cases} \tag{13}$$

where T_{3x} and x ∈ (1,2,3,4,5,6,7) represent the third harmonic electromagnetic compensated torque.

The compensation torque can be simplified further as follows by adding Eqs. 12, 13 and utilizing the sum and difference formula:

$$\begin{cases} T_{\sin\theta} = \frac{5P}{4}\left(2\psi_1 B + 3\psi_3 B - \frac{18{\psi_3}^2}{\psi_1}A\right)\sin\theta \\ T_{\sin 2\theta} = \frac{5P}{4}\left\{\left[(L_{d1}-L_{q1}) + (L_{d3}-L_{q3})\frac{9\psi_3^2}{\psi_1^2}\right]AB - 6\psi_3 C\right\} \\ T_{\sin 3\theta=}\frac{15P}{4}\psi_3(2A-B)\sin 3\theta \end{cases} \tag{14}$$

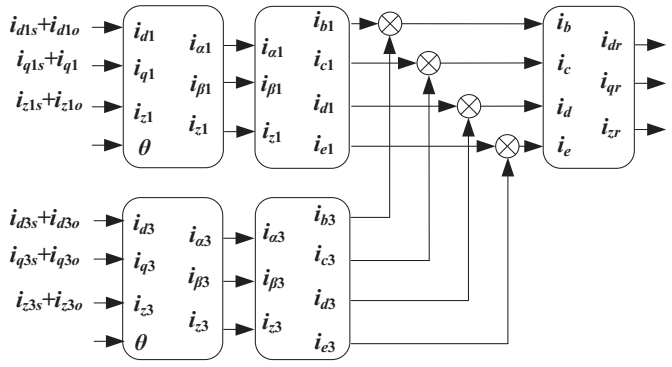

Fig. 3. Schematic of fault-tolerant reference currents generation under Phase-A short-circuit.

It is evident from Eq. 14 that first-, second-, and third-order ripples are present in the compensation torque. These can be utilized to counteract the torque ripple caused by the short-circuit current. To remove the output torque ripple, the amplitudes of the reference currents in the *d-q* axis can be obtained as follows by combining Eqs. 9, 14:

$$A = \frac{6\psi_1^2 + 6\psi_1\psi_3}{10\psi_1^2 + 15\psi_1\psi_3 - 45\psi_3^2} i_{sc},\ B = 2A - 0.8i_{sc},$$
$$C = \frac{AB}{6\psi_3}\left[(L_{d1} - L_{q1}) + (L_{d3} - L_{q3})\frac{9\psi_3^2}{\psi_1^2}\right] \tag{15}$$

The fault-tolerant currents can be obtained for the short-circuit fault condition by combining the suppression currents for phase-loss and the compensation currents for the short-circuit current. The suppression currents and compensation currents are allocated in the rotating coordinate system and superimposed on the natural coordinate system. Then, the fault-tolerant reference currents can be obtained by transforming the superimposed currents into the synchronous rotating coordinate in the fundamental space. The specific generation process of the fault-tolerant reference currents is shown in Fig. 3. By utilizing the fault-tolerant reference currents, the adverse effects of phase-loss and the short-circuit current can be offset. Thus, the motor can achieve disturbance-free operation with a smooth torque output under a short-circuit fault.

It is noteworthy that this fault-tolerant strategy can also be applied to sinusoidal back-EMF motors without additional calculation except for setting Ψ_3 to zero. Meanwhile, the transient process of the phase short-circuit is also considered because the short-circuit current is monitored in real-time. Then, the fault-tolerant currents would adjust automatically with i_{sc}.

3. Current tracking under fault condition

As shown in Eqs. 8, 11, the suppression currents and compensation currents contain cosine and sine components. Therefore, the synthetic fault-tolerant reference currents should also become AC quantities in the fundamental synchronous rotating coordinate. Hence, a deadbeat current prediction method is developed for the five-phase FTPMSM-TEMF to track these AC signals. The stator voltage equation of the motor can be expressed as:

$$\boldsymbol{U}_s = \boldsymbol{R}_s\boldsymbol{I}_s + \frac{d}{dt}(\boldsymbol{L}_s\boldsymbol{I}_s + \boldsymbol{\psi}_s) \tag{16}$$

where $\boldsymbol{U}_s$ and $\boldsymbol{I}_s$ represent the stator voltage and current matrix, respectively; $\boldsymbol{R}_s$ is the stator resistance matrix; and $\boldsymbol{\Psi}_s$ and $\boldsymbol{L}_s$ denote the PM flux linkage matrix and inductance matrix, respectively.

By using Clarke and Park transformation as shown in Eqs. 1, 2, and omitting the zero-sequence components, the stator voltage expression under the fault condition in the fundamental space can be obtained as:

$$\begin{cases} u_{d1} = R_s i_{d1} - \omega L_{q1} i_{q1} + L_{d1}\frac{di_{d1}}{dt} \\ u_{q1} = R_s i_{q1} + \omega L_{d1} i_{d1} + L_{q1}\frac{di_{q1}}{dt} + \omega\psi_1 \\ u_{z1} = R_s i_{z1} + L_{z1}\frac{di_{z1}}{dt} + 3\omega\psi_3\cos(3\theta) \end{cases} \tag{17}$$

where L_{d1} and L_{q1} are the inductances in a fundamental synchronous rotating coordinate, L_{z1} is the leakage inductance, R_s represents the stator resistance, u_{d1} and u_{q1} denote the stator voltage in a fundamental synchronous rotating coordinate, and u_{z1} is the third harmonic in a fundamental synchronous rotating coordinate.

It can be observed that Eq. 17 is a continuous equation. Using Euler's forward discretization method and based on Eq. 17, the continuity equation can be transformed into a discrete equation as shown in Eq. 18. It contains the relationship between the stator voltage and current in a constant order:

$$\begin{cases} i_{d1}(k+1) = (1 - \frac{R_s T_s}{L_{d1}})i_{d1}(k) + \omega\frac{L_{q1}T_s}{L_{d1}}i_{q1}(k) + \frac{T_s}{L_{d1}}u_{d1}(k) \\ i_{q1}(k+1) = -\omega\frac{L_{d1}T_s}{L_{q1}}i_{d1}(k) + (1 - \frac{R_s T_s}{L_{q1}})i_{q1}(k) + \frac{T_s}{L_{q1}}u_{q1}(k) - \frac{\omega\psi_1 T_s}{L_{q1}} \\ i_{z1}(k+1) = (1 - \frac{R_s T_s}{L_{z1}})i_{z1}(k) + \frac{T_s}{L_{z1}}u_{z1}(k) - \frac{3\omega\psi_3\cos(3\theta)T_s}{L_{z1}} \end{cases} \tag{18}$$

where T_s is the sample period; $i_{d1}(k)$, $i_{q1}(k)$, and $i_{z1}(k)$ represent the instantaneous currents in the fundamental synchronous rotating coordinate at the present instant; $u_{d1}(k)$, $u_{q1}(k)$, and $u_{z1}(k)$ denote the stator voltage in the fundamental synchronous rotating coordinate, which are performed in the present control period; and $i_{d1}(k+1)$, $i_{q1}(k+1)$, and $i_{z1}(k+1)$ are the predicted currents in the next sample time.

It is evident from Eq. 18 that when different voltage vectors are applied at the present instant, the corresponding predicted currents in the next sampling time would be generated.

Suppose $i_{d1}(k+1)$, $i_{q1}(k+1)$, and $i_{z1}(k+1)$ are equal to the fault-tolerant reference currents i_{dr}, i_{qr}, and i_{zr}. Combined with the feedback currents $i_{d1}(k)$, $i_{q1}(k)$, and $i_{z1}(k)$, the values of the voltages $u_{d1}(k)$, $u_{q1}(k)$, and $u_{z1}(k)$ in the current control period can be obtained according to Eq. 18. These can be considered as the fault-tolerant reference voltages u_{dr}, u_{qr}, and u_{zr}. The discrete equation Eq. 18 can be rewritten in a matrix form as shown in Eq. 19. It is evident that unlike the PI controller, the proposed method is not dependent on whether the currents are AC signals or not:

$$\begin{bmatrix} u_{dr} \\ u_{qr} \\ u_{zr} \end{bmatrix} = \begin{bmatrix} R_s - \frac{L_{d1}}{T_s} & -\omega L_{q1} & 0 \\ \omega L_{d1} & R_s - \frac{L_{q1}}{T_s} & 0 \\ 0 & 0 & R_s - \frac{L_{z1}}{T_s} \end{bmatrix} \begin{bmatrix} i_{d1}(k) \\ i_{q1}(k) \\ i_{z1}(k) \end{bmatrix} + \begin{bmatrix} \frac{L_{d1}}{T_s} & 0 & 0 \\ 0 & \frac{L_{q1}}{T_s} & 0 \\ 0 & 0 & \frac{L_{z1}}{T_s} \end{bmatrix} \begin{bmatrix} i_{dr} \\ i_{qr} \\ i_{zr} \end{bmatrix} + \begin{bmatrix} 0 \\ \omega\psi_1 \\ 3\omega\psi_3\cos 3\theta \end{bmatrix} \tag{19}$$

The fault-tolerant voltage references in the synchronous rotating coordinate can be obtained according to Eq. 19. A block diagram of the control system is presented in Fig. 4. It is shown that Eq. 19 can replace the PI controller to convert the reference currents into voltage under the fault condition.

CPWM is more flexible and convenient than conventional space pulse width modulation (SPWM) and space vector pulse width modulation (SVPWM) techniques. The vector distribution, sector assessment, and operation time of different vectors can be omitted while using CPWM. It can save calculation steps and implement these more conveniently in the digital controller. The speed is controlled by the speed closed-loop, and the current is controlled by the deadbeat current prediction method. The closed-loop of the current is established by combining the reference currents and sampling currents.

4. Experimental results

An experimental platform is conducted to verify the effectiveness of the proposed fault-tolerant strategy and deadbeat current predictive

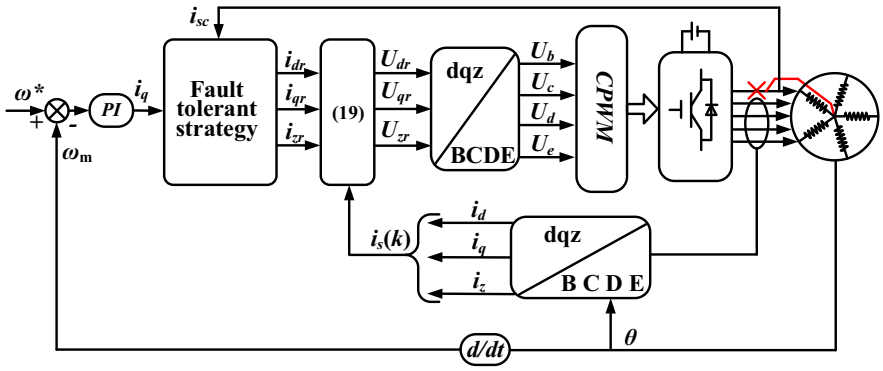

Fig. 4. Block diagram of proposed fault-tolerant control system under Phase-A short-circuit.

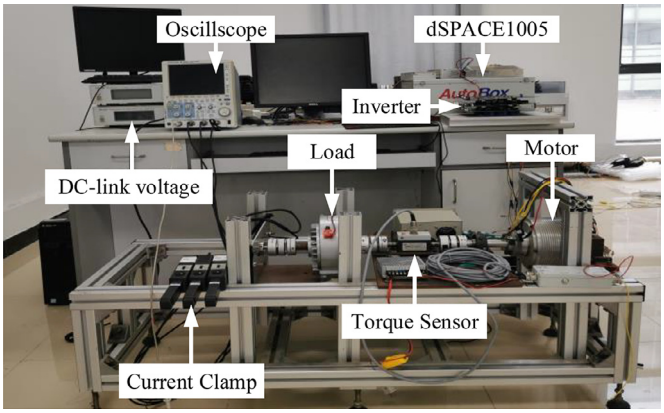

Fig. 5. Experimental test platform.

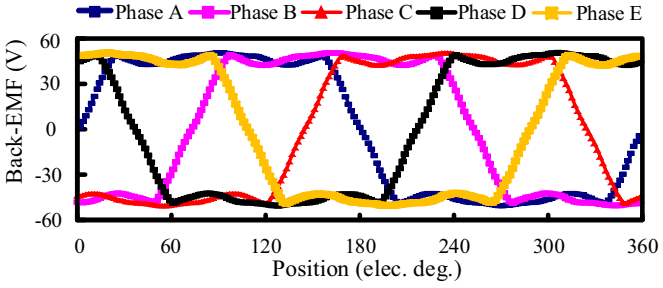

Fig. 6. Back-EMFs of healthy phases.

algorithm (see Fig. 5). The test platform is based on an in-wheel five-phase PM motor, five-phase half-bridge inverter, and magnetic powder brake as the load. The proposed fault-tolerant algorithm of the five-phase motor is developed and implemented in the dSPACE1005 controller. The motor torque is measured by a high-precision torque transducer (T20WN/20NM), where the cut-off frequency is 200 Hz. The frequency of insulated gate bipolar transistors (IGBTs) is fixed at 10 kHz, the sample rate of the current sensor is 10 kHz, and the direct current (DC) power is 50 V. In the experiment, the phase short-circuit fault condition is replicated by controlling the electric relay manually so that Phase A of the motor can be connected to the neutral point.

Fig. 6 shows the measured five back-EMF curves. The fast Fourier transform of the measured back-EMF data is carried out to obtain its frequency components. It is observed that the motor back-EMF contains 20% of the third harmonic. The motor parameters are listed in Table 1.

The reluctance torque in the motor magnetic circuit is marginal owing to the structure of fractional slot concentrated winding [33]. Meanwhile, it can be mentioned that the difference between L_{d1} and L_{q1} is 0.3 mH. Then, the theoretical reluctance torque is 0.004 Nm, which can be omitted.

Table 1
Motor parameters

Parameters	Value
Slot number	20
Pole-pairs	9
Rated current (A)	10.8
Rated speed (r/min)	1000
Fundamental permanent magnet flux linkage (Wb)	0.0411
Third harmonic permanent magnet flux linkage (Wb)	0.0033
Phase inductance (mH)	1.634
Fundamental *d*-axis inductance (mH)	0.9323
Fundamental *q*-axis inductance (mH)	1.2614
Leakage inductance (mH)	0.23

4.1. Fault-tolerant operation test

The behavior of the proposed fault-tolerant control under short-circuit of Phase A is first analyzed. To protect the devices, the motor is operated at a constant speed of 400 r/min (60 HZ), and the load torque is 1.57 Nm.

Fig. 7 shows the phase currents and torque waveforms around the fault occurrence. It is evident that when the short-circuit fault occurs, the torque ripple increases significantly, attaining 177.71%. Meanwhile, the amplitudes of the remaining healthy currents increase abruptly and exceed the rated current by approximately 50.65%. The torque ripples are suppressed significantly (approximately 75.63%) by the using of the proposed fault-tolerant strategy. This verifies the effectiveness and feasibility of the proposed fault-tolerant method.

The amplitudes of torque ripples in different harmonic orders under normal, fault, and fault-tolerant conditions are shown in Fig. 8 for 400 r/min and 1.75 Nm. It is evident that the second-order torque ripple increases significantly from 0.037 Nm to 2.503 Nm when the motor runs under fault conditions. However, the amplitude of the second-order torque pulsation decreases by 86.58% when the fault-tolerant strategy is implemented. This is favorable to the disturbance-free operation of the motor under Phase-A short-circuit conditions. Because the prototype is not a complete trapezoidal back-EMF as shown in Fig. 6, a few pulsations appear in the results of the fault-tolerance experiment. It is also evident that the fourth-order ripple is significantly less than the second-order ripple in the fault condition. This is because the first and third pulsation of the short-circuit current would interact with the back-EMF and eventually produce mainly second pulsations and a few fourth torque ripples. Meanwhile, owing to the initial phase, the fourth torque ripple would be offset partly by the fourth torque ripples generated by the loss of Phase A. Thus, the torque ripple of the fourth-order is significantly less than that of the second in case of fault.

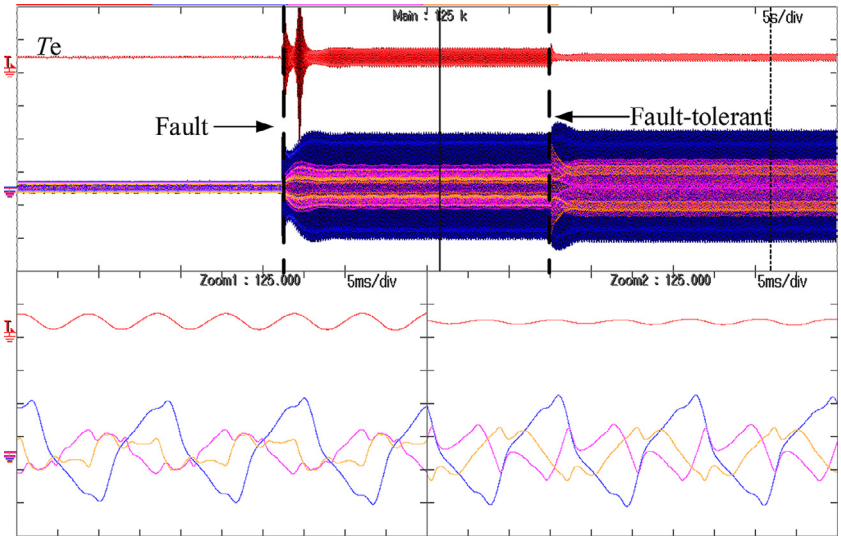

Fig. 7. Torque and current waveforms under the A-phase fault Pre-and post-fault-tolerant operation. T_e is scaled to 5 Nm/div, phase currents are scaled to 10 A/div. The average torque T_e is 1.57 Nm. The torque ripple under fault condition is 177.71%, while the torque ripple under fault-tolerant condition is 43.31%. The short-circuit current (blue line) is 16.52 A. The current of phase B (pink line) per- and post- fault is 10.47 A and 10.85 A respective. The current of phase C (orange line) per- and post- fault is 10.53 A and 13.88 A respective.

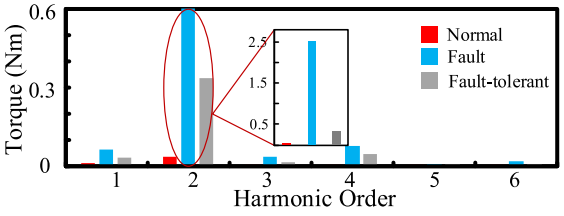

Fig. 8. Amplitudes of torque ripples of different orders.

The thermal resistance network of the fault condition is given in Fig. 9a. The temperature variation trend of the winding and PM of the motor are displayed in Fig. 9b, c. These are simulated by a lumped parameter thermal network. It is evident that the motor temperature increases substantially in 2000 s. However, after 8000 s, the temperature tends to stabilize and does not increase further significantly. It is evident that in the steady-state, the temperature of the fault is approximately 30% higher than normal. N35UH can be selected as the PM material to prevent irreversible demagnetization. This is because the maximum operating temperature of this type of PM is 180 °C. Meanwhile, the winding temperature can be suppressed by cooling measures such as cooling

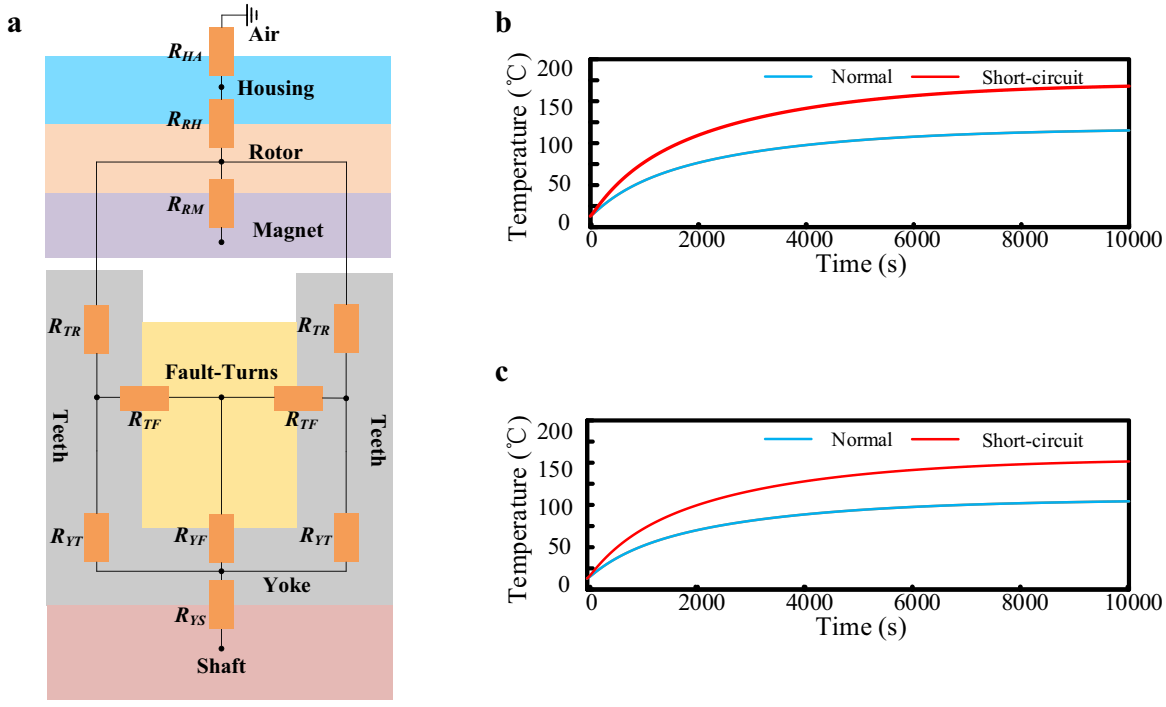

Fig. 9. Thermal analysis of five-phase FTPMSM-TEMF. (a) Lumped parameter thermal network. (b) Temperature of winding. (c) Temperature of PM.

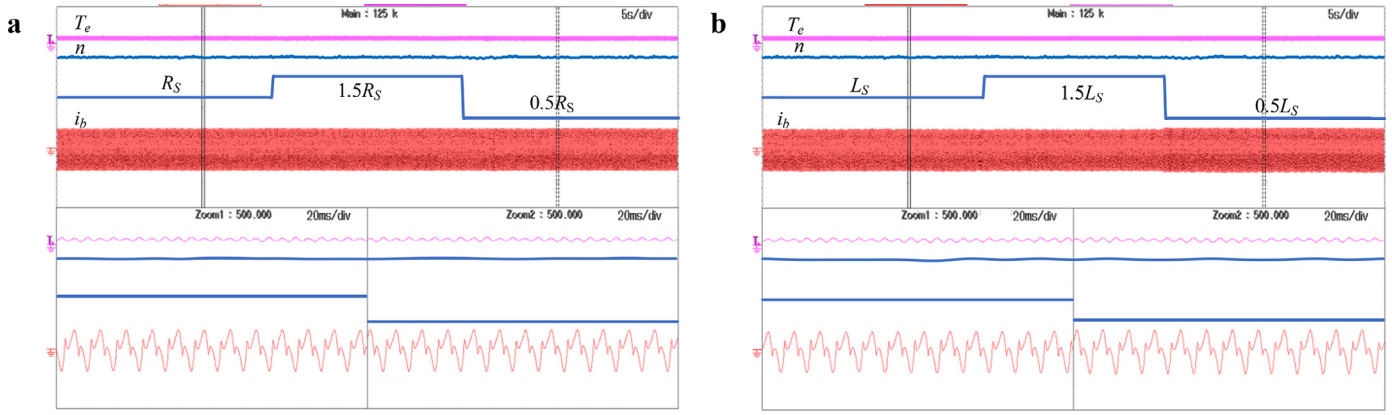

Fig. 10. Parameter sensitivity analysis of proposed methods under fault-tolerant conditions. (a) Stator resistance. (b) *dq*-axis inductance.

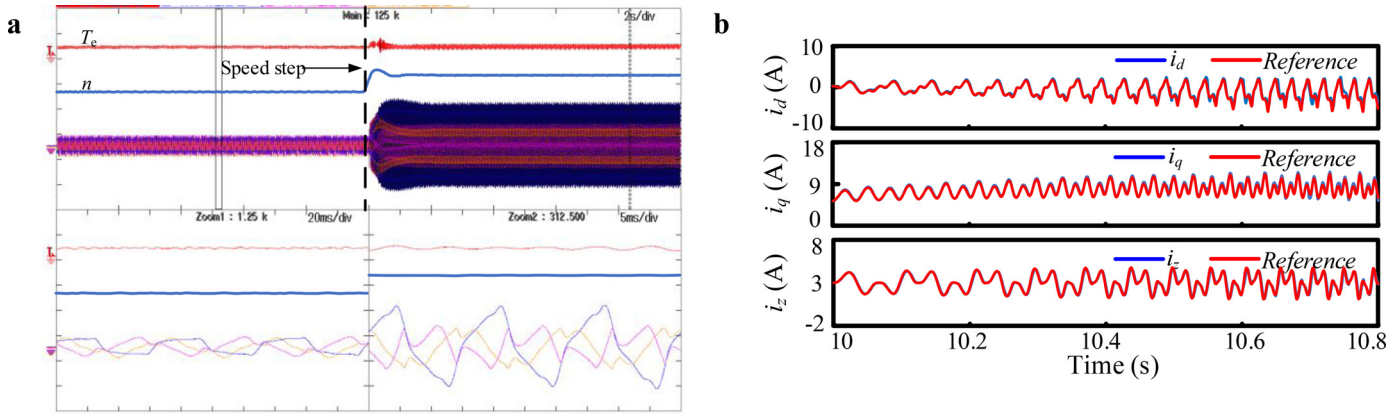

Fig. 11. Fault-tolerant operation under load step. (a) Currents and torque response. (b) *d-q-z* current response. The speed is 400 r/min, and the average torque T_e is step from 0 Nm to 1.68 Nm. The short-circuit current (blue line) is 16.5 A. The current of phase B (pink line) is step from 7.26 A to 11.16 A. The current of phase C (orange line) is step from 7.79 A to10.89 A.

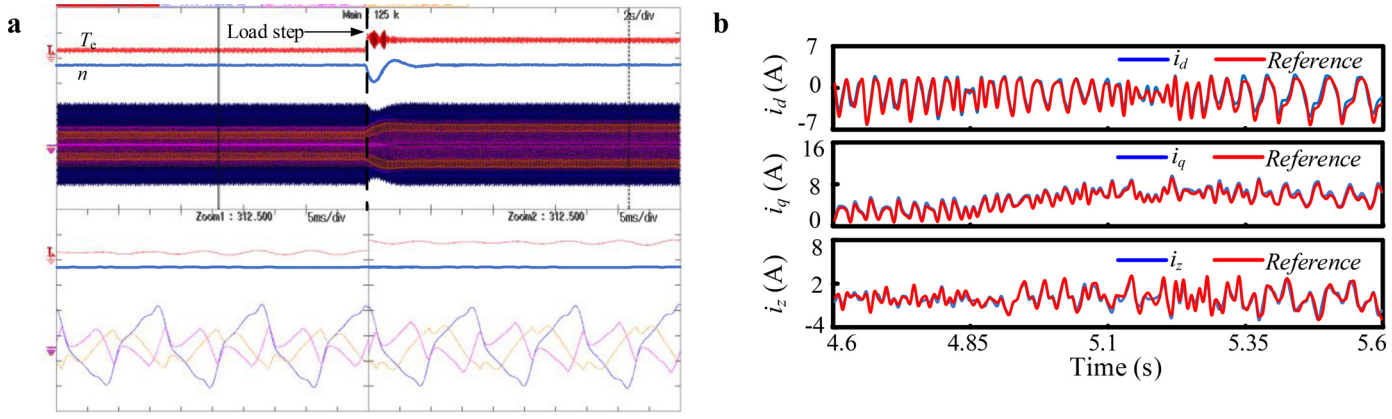

Fig. 12. Fault-tolerant operation under speed step. (a) Currents and torque response. (b) *d-q-z* current response. The average torque T_e is 1.74 Nm, and the speed is step from 100 r/min to 400 r/min. The short-circuit current (blue line) is step from 5.23 A to 17.05A. The current of phase B (pink line) is step from 5.30 A to 10.98 A. The current of phase C (orange line) is step from 6.55 A to 13.77 A.

fan and oil-cooling. In this case, the temperature can be endured, and the motor can maintain the output capacity for a long time under the fault-tolerant operation.

4.2. Parameter sensitivity analysis

The deadbeat method proposed in the paper relies on the precise motor parameters that are utilized to obtain the required fault-tolerant reference voltages. However, it is difficult to accurately determine a parameter in actual application because of the variation in noise or temperature. Thus, it is necessary to evaluate the parameter sensitivity of the proposed deadbeat current prediction method.

In this test, the stator resistance and the inductance would increase by 150% and then, reduce to 50% after a few seconds. The experimental results are shown in Fig. 10. It is evident that the operational performance is almost unaffected by the variations in stator resistance. When the inductance decreases, the current amplitude increases accordingly. However, the actual speed and torque are maintained. This implies that the proposed deadbeat method has good robustness.

4.3. Dynamic performances under fault-tolerant operation

Several tests are performed under fault-tolerant conditions to evaluate the dynamic response of the proposed fault-tolerant control and deadbeat current tracking strategy.

Fig. 11a, b shows the experimental speed, current response, and current tracking capability under a speed step at 10 s. The reference speed is varied from 100 to 400 r/min. It can be observed that in the case of the fault-tolerant condition, when the speed step occurs, the magnitude of the short-circuit current i_{sc} is increased abruptly, and the reference currents at the fundamental synchronous rotating coordinate are adjusted rapidly by the speed closed-loop PI controller and the fault-tolerant strategy. The actual speed is also switched rapidly. Meanwhile, the actual currents can accurately track the fault-tolerant reference currents during the speed-step process. It can be observed that the motor recovers to a stable condition after a short adjustment time.

Fig. 12a, b shows a test to further verify that the proposed fault-tolerant strategy maintains high performance and robustness in terms of load step. The transient states involve the application of one-step transitions of the load from 0 to 1.68 Nm to the motor. Throughout the adjustment process, the reference currents i_q adjust rapidly, and the actual currents demonstrate a stable tracking performance. When the load is switched, negligible variation occurs in the amplitude of the short-circuit current, and the amplitudes of the remaining healthy phase currents increase corresponding to the load torque. It can be observed that after a short adjustment, the motor enters a new equilibrium state.

It can be concluded from the above analysis that the disturbance-free operation under a short-circuit fault can be obtained using the proposed fault-tolerant strategy. Meanwhile, the alternating reference current signal in the fundamental synchronous rotating coordinate system can also be tracked effectively by the deadbeat model current prediction method.

5. Conclusion

This paper proposes a new post-fault control method for a five-phase PM motor with trapezoidal back-EMF under short-circuit conditions. Based on the decoupling model, the torque ripple caused by phase-loss is fully utilized to offset the influence of the short-circuit current and thereby, realize undisturbed operation. Because the fault-tolerant reference currents are AC signals in a rotating coordinate system, the mode of deadbeat current prediction control for five-phase FTPMSM-TEMF is established to track the reference currents. The proposed post-fault control method and current tracking method are verified experimentally. Both the results demonstrate that the proposed post-fault control method can offset torque ripple successfully and that the deadbeat currents predictive control can track the alternating currents effectively.

6. Appendix

6.1. Expression for torque in the fundamental synchronous rotating coordinate

The fundamental reduced-order Clarke and Park transformation has the following relationship:

$$\boldsymbol{T} = \boldsymbol{T}^{A}_{park1} * \boldsymbol{T}^{A}_{clarke1} \tag{20}$$

$$\boldsymbol{T}^{A}_{clarke1}{}^{-1} = \boldsymbol{T}^{A}_{clarke1}{}^{T} * A = \frac{5}{2} * \boldsymbol{T}^{A}_{clarke1}{}^{T} * \begin{bmatrix} 2 & 0 & 0 & 5 \\ 0 & 1 & 0 & 0 \\ 0 & 0 & 1 & 0 \\ 5 & 0 & 0 & 15 \end{bmatrix}$$

It is evident from Eq. 3 that the torque expression can be divided into two parts: the inductance part and PM part.

According to reduced-order Clarke and Park transformation, the inductance part of the torque expression can be obtained as:

$$\begin{aligned} T_{ind} &= \frac{1}{2} P \boldsymbol{I}_s^T \frac{\partial \boldsymbol{L}_s}{\partial \theta} \boldsymbol{I}_s = \frac{1}{2} P (\boldsymbol{T}^{-1} \boldsymbol{i}_{dq})^T \frac{\partial \boldsymbol{T} \boldsymbol{L}_{dq} \boldsymbol{T}^{-1}}{\partial \theta} (\boldsymbol{T}^{-1} \boldsymbol{i}_{dq}) \\ &= \frac{5P}{2} (L_{d1} - L_{q1}) i_{d1} i_{q1} \end{aligned} \tag{21}$$

The PM part of the torque expression Eq. 3 can be expressed as:

$$\begin{aligned} T_{per} &= P * \boldsymbol{I}_S^T * \frac{\partial \boldsymbol{\psi}_s}{\partial \theta} = P * \left[(\boldsymbol{T}^{A}_{park1} * \boldsymbol{T}^{A}_{clarke1})^{-1} * \boldsymbol{i}_{dq} \right]^T * \frac{\partial (\boldsymbol{T}^{A}_{park1} * \boldsymbol{T}^{A}_{clarke1})^{-1}}{\partial \theta} * \boldsymbol{\psi}_{dq} \\ &= P * \left[\boldsymbol{T}^{A}_{park1} * \boldsymbol{T}^{A}_{clarke1} * \boldsymbol{i}_{dq} \right]^T * \left[(\boldsymbol{T}^{A}_{park1} * \boldsymbol{T}^{A}_{clarke1})^{-1} * \frac{\partial \boldsymbol{\psi}_{dq}}{\partial \theta} + \frac{\partial (\boldsymbol{T}^{A}_{park1} * \boldsymbol{T}^{A}_{clarke1})^{-1}}{\partial \theta} * \boldsymbol{\psi}_{dq} \right] \\ &= P * \left[\boldsymbol{T}^{A}_{clarke1}{}^{T} * A * \boldsymbol{T}^{A}_{park1}{}^{-1} * \boldsymbol{i}_{dq} \right]^T * \left[(\boldsymbol{T}^{A}_{park1} * \boldsymbol{T}^{A}_{clarke1})^{-1} * \frac{\partial \boldsymbol{\psi}_{dq}}{\partial \theta} + \frac{\partial (\boldsymbol{T}^{A}_{park1} * \boldsymbol{T}^{A}_{clarke1})^{-1}}{\partial \theta} * \boldsymbol{\psi}_{dq} \right] \\ &= P * \left[\boldsymbol{i}_{dq}^T * \boldsymbol{T}^{A}_{park1} * A * \boldsymbol{T}^{A}_{clarke1} \right] * \left[\boldsymbol{T}^{A}_{clarke1}{}^{-1} * \boldsymbol{T}^{A}_{park1}{}^{-1} * \frac{\partial \boldsymbol{\psi}_{dq}}{\partial \theta} + \frac{\partial \boldsymbol{T}^{A}_{clarke1}{}^{-1} * \boldsymbol{T}^{A}_{park1}{}^{-1}}{\partial \theta} * \boldsymbol{\psi}_{dq} \right] \\ &= P * \boldsymbol{i}_{dq}^T * \left[\boldsymbol{T}^{A}_{park1} * A * \boldsymbol{T}^{A}_{park1}{}^{-1} * \frac{\partial \boldsymbol{\psi}_{dq}}{\partial \theta} + \boldsymbol{T}^{A}_{park1} * A * \frac{\partial \boldsymbol{T}^{A}_{park1}{}^{-1}}{\partial \theta} * \boldsymbol{\psi}_{dq} \right] \\ &= P * \boldsymbol{i}_{dq}^T * T_{per1} + T_{per2} \end{aligned} \tag{22}$$

where T_{per1} and T_{per2} can be calculated as:

$$\begin{aligned} T_{per1} &= \boldsymbol{T}^{A}_{park1} * A * \boldsymbol{T}^{A}_{park1}{}^{-1} * \frac{\partial \boldsymbol{\psi} dq}{\partial \theta} \\ &= \boldsymbol{T}^{A}_{park1} * \frac{5}{2} * \begin{bmatrix} 2 & 0 & 0 & 5 \\ 0 & 1 & 0 & 0 \\ 0 & 0 & 1 & 0 \\ 5 & 0 & 0 & 15 \end{bmatrix} * \boldsymbol{T}^{A}_{park1}{}^{-1} * \begin{bmatrix} 0 \\ 0 \\ 3\psi_3 \cos 3\theta \\ \frac{1}{5}\psi_1 \sin\theta + \frac{3}{5}\psi_3 \sin 3\theta \end{bmatrix} \\ &= \frac{5}{2} * \begin{bmatrix} \psi_1 \sin\theta \cos\theta + 3\psi_3 \sin 3\theta \cos\theta \\ -\psi_1 \sin^2\theta - 3\psi_3 \sin 3\theta \sin\theta \\ 3\psi_3 \cos 3\theta \\ 3\psi_1 \sin\theta + 9\psi_3 \sin 3\theta \end{bmatrix} \end{aligned} \tag{23}$$

$$\begin{aligned} T_{per2} &= \boldsymbol{T}^{A}_{park1} * A * \frac{\partial \boldsymbol{T}^{A}_{park1}{}^{-1}}{\partial \theta} * \boldsymbol{\psi}_{dq} \\ &= \boldsymbol{T}^{A}_{park1} * \frac{5}{2} * \begin{bmatrix} 2 & 0 & 0 & 5 \\ 0 & 1 & 0 & 0 \\ 0 & 0 & 1 & 0 \\ 5 & 0 & 0 & 15 \end{bmatrix} * \frac{\partial \boldsymbol{T}^{A}_{park1}{}^{-1}}{\partial \theta} * \begin{bmatrix} \psi_1 \\ 0 \\ \psi_3 \sin 3\theta \\ -\frac{1}{5}\psi_1 \cos\theta - \frac{1}{5}\psi_3 \cos 3\theta \end{bmatrix} \\ &= \frac{5}{2} * \begin{bmatrix} -\psi_1 \sin\theta \cos\theta \\ \psi_1 + \psi_1 \sin^2\theta \\ 0 \\ 0 \end{bmatrix} \end{aligned} \tag{24}$$

By substituting Eqs. 23, 24 into Eq. 22, the PM torque can be expressed as:

$$\begin{aligned} T_{per} &= P * \boldsymbol{i}_{dq}^T * T_{per1} + T_{per2} \\ &= \frac{5}{2} * P * \begin{bmatrix} i_{d1} & i_{q1} & i_{z3} & i_{z0} \end{bmatrix} * \begin{bmatrix} 3\psi_3 \sin 3\theta \cos\theta \\ \psi_1 - 3\psi_3 \sin 3\theta \sin\theta \\ 3\psi_3 \cos 3\theta \\ 3\psi_1 \sin\theta + 9\psi_3 \sin 3\theta \end{bmatrix} \\ &= \frac{5}{2} * P * \left[\psi_1 i_{q1} + 3\psi_3 (i_{d1} \sin 3\theta \cos\theta - i_{q1} \sin 3\theta \sin\theta + i_{z1} \cos 3\theta) \right] \\ &= \frac{5}{2} * P * \left\{ \psi_1 i_{q1} + 3\psi_3 \left[0.5 i_{d1} (\sin 4\theta + \sin 2\theta) + 0.5 i_{q1} (\cos 4\theta - \cos 2\theta) + i_{z1} \cos 3\theta \right] \right\} \end{aligned} \tag{24}$$

By substituting Eqs. 21, 24 into Eq. 3, the electromagnetic torque at the fundamental synchronous rotating coordinate can be obtained as shown in Eq. 5.

6.2. Inductance component in the fundamental synchronous rotating coordinate

$$\begin{bmatrix} L_{d1} & & & \\ & L_{q1} & & \\ & & L_{z1} & \\ & & & L_0 \end{bmatrix}$$

$$= (\boldsymbol{T}^{A}_{park1} * \boldsymbol{T}^{A}_{clark1}) \begin{bmatrix} L_{BB} & L_{BC} & L_{BD} & L_{BE} \\ L_{CB} & L_{CC} & L_{CD} & L_{CE} \\ L_{DB} & L_{DC} & L_{DD} & L_{DE} \\ L_{EB} & L_{EC} & L_{ED} & L_{EE} \end{bmatrix} (\boldsymbol{T}^{A}_{park1} * \boldsymbol{T}^{A}_{clark1})^{-1} \tag{25}$$

$$\begin{bmatrix} L_{d3} & & & \\ & L_{q3} & & \\ & & L_{z3} & \\ & & & L_0 \end{bmatrix}$$

$$= (\boldsymbol{T}^{A}_{park3} * \boldsymbol{T}^{A}_{clark3}) \begin{bmatrix} L_{BB} & L_{BC} & L_{BD} & L_{BE} \\ L_{CB} & L_{CC} & L_{CD} & L_{CE} \\ L_{DB} & L_{DC} & L_{DD} & L_{DE} \\ L_{EB} & L_{EC} & L_{ED} & L_{EE} \end{bmatrix} (\boldsymbol{T}^{A}_{park3} * \boldsymbol{T}^{A}_{clark3})^{-1}$$

where the value of the inductance matrix is obtained through finite element simulation.

6.3. Detailed expression of the phase fault-tolerant currents in the natural coordinate system

$$\begin{aligned} i_b &= 1.382i_{q1}\cos(\theta - 0.2\pi) + 1.176i_{q1}\cos(3\theta + 0.9\pi) + 0.7205i_{sc}\cos(2\theta - 0.22\pi) \\ &+ 0.0364i_{sc}\cos(2\theta - 0.78\pi) + 0.1735i_{sc}\cos(4\theta + 0.22\pi) + 0.1152i_{sc} \\ i_c &= 1.382i_{q1}\cos(\theta - 0.8\pi) + 1.561i_{q1}\cos(3\theta - 0.25\pi) + 0.62i_{sc}\cos(2\theta - 0.75\pi) \\ &+ 0.0314i_{sc}\cos(2\theta - 0.15\pi) + 0.1493i_{sc}\cos(4\theta + 0.85\pi) - 0.1152i_{sc} \\ i_d &= 1.382i_{q1}\cos(\theta + 0.8\pi) + 1.561i_{q1}\cos(3\theta + 0.25\pi) + 0.62i_{sc}\cos(2\theta + 0.75\pi) \\ &+ 0.0314i_{sc}\cos(2\theta + 0.15\pi) + 0.1493i_{sc}\cos(4\theta - 0.85\pi) - 0.1152i_{sc} \\ i_e &= 1.382i_{q1}\cos(\theta + 0.2\pi) + 1.176i_{q1}\cos(3\theta - 0.9\pi) + 0.7205i_{sc}\cos(2\theta + 0.22\pi) \\ &+ 0.0364i_{sc}\cos(2\theta + 0.78\pi) + 0.1735i_{sc}\cos(4\theta - 0.22\pi) + 0.1152i_{sc} \end{aligned} \tag{26}$$

Declaration of Competing Interest

The authors declared that they have no conflict of interest in this work.

Acknowledgments

This work was supported in part by the National Natural Science Foundation of China (Grants No. 52077097, 52025073, and 51991383), in part by the Natural Science Research Project of Higher Education Institutions of Jiangsu Province (Grant No. 20KJA470003), and in part by the Priority Academic Program Development of Jiangsu Higher Education Institutions.

References

[1] K Wang, Z Gu, C Liu, et al., Design and analysis of five phase SPM machine considering third harmonic current injection, IEEE Trans. Energy Convers 33 (3) (2018) 1108–1117.
[2] A Salem, M. Narimani, A review on multiphase drives for automotive traction applications, IEEE Trans. Transport. Electrific 5 (4) (2019) 1329–1348.
[3] J Xu, Y Du, B Zhang, et al., Sensorless fault tolerant control with phase delay compensation for aerospace FTPMSM drives with phase open-circuit and short-circuit faults, IEEE Trans. Ind. Electron 68 (6) (2021) 4576–4585.
[4] D Ye, J Li, J Chen, et al., Study on steady-state errors for asymmetrical six-phase permanent magnet synchronous machine fault-tolerant predictive current control, IEEE Trans. Power Electron 35 (1) (2020) 640–651.
[5] C Xiong, H Xu, T Guan, et al., Fault-tolerant FOC for five-phase SPMSM with non-sinusoidal back EMF, IET Electr. Power Appl 13 (11) (2019) 1734–1742.
[6] G Liu, C Song, Q. Chen, FCS-MPC-based fault-tolerant control of five-phase IPMSM for MTPA operation, IEEE Trans. Power Electron 35 (3) (2020) 2882–2894.
[7] Q Chen, W Zhao, G Liu, et al., Extension of virtual-signal-injection-based MTPA control for five-phase IPMSM into fault-tolerant operation, IEEE Trans. Ind. Electron 66 (2) (2019) 944–955.
[8] B Tian, Q An, J Duan, et al., Decoupled modeling and nonlinear speed control for five-phase PM motor under single-phase open fault, IEEE Trans. Power Electron 32 (7) (2017) 5473–5486.
[9] G Liu, Z Lin, W Zhao, et al., Third harmonic current injection in fault-tolerant five-phase permanent-magnet motor drive, IEEE Trans. Power Electron 33 (8) (2018) 6970–6979.
[10] M Cheng, J Hang, J. Zhang, Overview of fault diagnosis theory and method for permanent magnet machine, Chinese J. Electr. Eng 1 (1) (2015) 21–36.
[11] R Sadeghi, H Samet, T. Ghanbari, Detection of stator short-circuit faults in induction motors using the concept of instantaneous frequency, IEEE Trans. Ind. Informat 15 (8) (2019) 4506–4515.
[12] L Xiao, H Sun, F Gao, et al., A new diagnostic method for winding short-circuit fault for srm based on symmetrical component analysis, Chinese J. Electr. Eng 4 (1) (2018) 74–82.
[13] Z Ullah, J. Hur, Analysis of inter-turn-short fault in an FSCW IPM type brushless motor considering effect of control drive, IEEE Trans. Ind. Appl 56 (2) (2020) 1356–1367.
[14] A Jafari, J Faiz, M. Jarrahi, A simple and efficient current-based method for interturn fault detection in BLDC motors, IEEE Trans. Ind. Informat 17 (4) (2020) 2707–2715.
[15] Z Yin, Y Sui, P Zheng, et al., Short-circuit fault-tolerant control without constraint on d-Axis armature magnetomotive force for five-phase PMSM, IEEE Trans. Ind. Electron. (2020), doi:10.1109/TIE.2021.3084172.
[16] W Zhao, C Gu, Q Chen, et al., Remedial phase-angle control of a five-phase fault–tolerant permanent-magnet vernier machine with short-circuit fault, CES Trans. on Electrical Machines and Systems 1 (1) (2017) 83–88.
[17] H Zhou, G Liu, W Zhao, et al., Dynamic performance improvement of five-phase permanent-magnet motor with short-circuit fault, IEEE Trans. Ind. Electron 65 (1) (2018) 145–155.
[18] F Wu, C Tong, Y Sui, et al., Influence of third harmonic back EMF on modeling and remediation of winding short circuit in a multiphase PM machine with FSCWs, IEEE Trans. Ind. Electron 63 (10) (2016) 6031–6041.
[19] Y Wang, L Geng, W Hao, et al., Improved control strategy for fault-tolerant flux-switching permanent-magnet machine under short-circuit condition, IEEE Trans. Power Electron 34 (5) (2019) 4536–4557.
[20] A Mohammadpour, L. Parsa, in: Post-fault control technique for multiphase PM motor drives under short-circuit faults, 2013, pp. 817–822, doi:10.1109/APEC.2013.6520304. Proc. 2013 28th Annu, IEEE Appl. Power Electron. Conf. Expo.
[21] A Mohammadpour, L. Parsa, Global fault-tolerant control technique for multiphase permanent-magnet machines, IEEE Trans. Ind. Appl 51 (1) (2015) 178–186.
[22] Bhaskar Sen, J. Wang, Stationary frame fault-tolerant current control of polyphase permanent-magnet machines under open-circuit and short-circuit faults, IEEE Trans. Power Electron 31 (7) (2016) 4684–4696.
[23] J Zhang, L Li, D.G Dorrell, et al., Modified PI controller with improved steady-state performance and comparison with PR controller on direct matrix converters, Chinese J. Electr. Eng 5 (1) (2019) 53–66.
[24] S.A Richter, Doncker R.W. De, Digital proportional-resonant (PR) control with anti-windup applied to a voltage-source inverter, in: Proc. 14th Eur.Conf. Power Electron, 2011, pp. 1–10.
[25] M.S.R Saeed, W Song, B Yu, et al., Low-complexity deadbeat model predictive current control with duty ratio for five-phase PMSM drives, IEEE Trans. Power Electron 35 (11) (2020) 12085–12099.
[26] C Xu, Z Han, S. Lu, Deadbeat predictive current control for permanent magnet synchronous machines with closed-form error compensation, IEEE Trans. Power Electron 35 (5) (2020) 5018–5030.
[27] X Li, S Zhang, C Zhang, et al., An improved deadbeat predictive current control scheme for open-winding permanent magnet synchronous motors drives with disturbance observer, IEEE Trans. Power Electron 36 (4) (2021) 4622–4632.
[28] X Wang, Z Wang, Z Xu, et al., Deadbeat predictive current control based fault-tolerant scheme for dual three-phase PMSM drives, IEEE J. Emerg. Sel. Top. Power Electron 9 (2) (2021) 1591–1604.
[29] Y Shi, J Wang, R Hu, et al., Electromagnetic and thermal behavior of a triple redundant 9-Phase PMASynRM with insulation deterioration fault, IEEE Trans. Ind. Appl 56 (6) (2020) 6374–6383.
[30] Q Chen, G Liu, W Zhao, et al., Design and comparison of two fault-tolerant interior-permanent-magnet motors, IEEE Trans. Ind. Electron 61 (12) (2014) 6615–6623.
[31] Z.Z. Wu, Z.Q. Zhu, H.L. Zhan, Comparative analysis of partitioned stator flux reversal PM machines having fractional-slot nonoverlapping and integer-slot overlapping windings, IEEE Trans. Energy Convers 31 (2) (2016) 776–788.
[32] J Hang, S Ding, X Ren, et al., Integration of interturn fault diagnosis and torque ripple minimization control for direct-torque-controlled SPMSM drive system, IEEE Trans. Power Electron 36 (10) (2021) 11124–11134.
[33] Q Chen, Y Yan, G Liu, et al., Design of a new fault-tolerant permanent magnet machine with optimized salient ratio and reluctance torque ratio, IEEE Trans. Ind. Electron 67 (7) (2020) 6043–6054.

Qian Chen received the B.Sc. and Ph.D. degrees from Jiangsu University, Zhenjiang, China, in 2009 and 2015, respectively, in electrical engineering and control engineering. He has been with Jiangsu University since 2015, where he is currently an Associate Professor in the School of Electrical Information Engineering. He is a Full Member of Sigma Xi, The Scientific Research Honor Society. From 2020 to 2021, he was a Visiting Professor with the Department of Electronic and Electrical Engineering, University of Sheffield, Sheffield, U.K. His current research interests include electric machine design, modeling, fault analysis, and intelligent control.

Jiabin Wang received the B.Eng. and M.Eng. degrees from the Jiangsu University of Science and Technology, Zhenjiang, China, in 1982 and 1986, respectively, and the Ph.D. degree from the University of East London, London, U.K., in 1996, all in electrical and electronic engineering. He is currently a Professor of electrical engineering with the University of Sheffield, Sheffield, U.K., where he was a Postdoctoral Research Associate from 1996 to 1997. From 1998 to 2001, he was a Senior Lecturer with the University of East London, London. His research interests include motion control and electromechanical energy conversion to electric drives for applications in automotive, renewable energy, household appliances, and aerospace sectors. Dr. Wang is a fellow of the IET.

Wenxiang Zhao received the B.Sc. and M.Sc. degrees from Jiangsu University, Zhenjiang, China, in 1999 and 2003, respectively, and the Ph.D. degree from Southeast University, Nanjing, China, in 2010, all in electrical engineering. He has been with Jiangsu University since 2003, where he is currently a Professor with the School of Electrical Information Engineering. From 2008 to 2009, he was a Research Assistant with the Department of Electrical and Electronic Engineering, University of Hong Kong, Hong Kong. From 2013 to 2014, he was a Visiting Professor with the Department of Electronic and Electrical Engineering, University of Sheffield, Sheffield, U.K. His current research interests include electric machine design, modeling, fault analysis, and intelligent control. He has authored and co-authored over 200 technical papers in these areas.